HAL
open science

Time-dependent electronic current densities in chiral molecules

Sucharita Giri, Alexandra Maxi Dudzinski, Jean Christophe Tremblay, Gopal Dixit

To cite this version:

Sucharita Giri, Alexandra Maxi Dudzinski, Jean Christophe Tremblay, Gopal Dixit. Time-dependent electronic current densities in chiral molecules. Physical Review A, 2020, 102 (6), pp.063103. 10.1103/PhysRevA.102.063103 . hal-02332717

HAL Id: hal-02332717

https://hal.univ-lorraine.fr/hal-02332717v1

Submitted on 11 Aug 2023

HAL is a multi-disciplinary open access archive for the deposit and dissemination of scientific research documents, whether they are published or not. The documents may come from teaching and research institutions in France or abroad, or from public or private research centers.

L'archive ouverte pluridisciplinaire **HAL**, est destinée au dépôt et à la diffusion de documents scientifiques de niveau recherche, publiés ou non, émanant des établissements d'enseignement et de recherche français ou étrangers, des laboratoires publics ou privés.

Time-dependent electronic current densities in chiral molecules

Sucharita Giri,[1,2] Alexandra Maxi Dudzinski,[2,3] Jean Christophe Tremblay,[2,4,*] and Gopal Dixit[1,†]
[1]*Department of Physics, Indian Institute of Technology Bombay, Powai, Mumbai 400076, India*
[2]*Institut für Chemie und Biochemie, Freie Universität Berlin, Takustraße 3, 14195 Berlin, Germany*
[3]*Institut NEEL CNRS/UGA UPR2940, 25 rue des Martyrs BP 166, 38042 Grenoble cedex 9, France*
[4]*Laboratoire de Physique et Chimie Théoriques, CNRS-Université de Lorraine, UMR 7019, ICPM, 1 Bd Arago, 57070 Metz, France*

(Received 1 October 2019; revised 14 December 2019; accepted 9 November 2020; published 4 December 2020)

The present work focuses on the conditions required to understand time-dependent ultrafast charge migration in oriented and floppy chiral molecules. Ultrashort linearly polarized laser pulses are used to drive an ultrafast charge migration process by the excitation of a small number of low-lying excited states from the ground electronic state of R- and S-epoxypropane. Control over electron dynamics is achieved by choosing the different orientations of the linearly polarized pulse. For oriented and floppy molecules, we find that the charge migration is different for enantiomers when the polarization of the pulse lies in the mirror plane defining the enantiomer pair, or when it is strictly perpendicular to it. Ultimately the choice of polarization of the linearly polarized pulse determines the properties of the charge migration process in the chiral molecules, i.e., the direction of the electronic current densities.

DOI: 10.1103/PhysRevA.102.063103

I. INTRODUCTION

Chirality, which can be defined as the geometric property of a molecule being nonsuperposable on its mirror image, is a general property observed in nature. Distinguishing and understanding the chirality of molecules is essential in a broad range of sciences. One example is the important role that homochirality plays in life on Earth [1–3]. Enantiomers—a pair of chiral molecules—possess similar physical properties but they show strong enantiomeric preference during chemical reactions. Therefore, detecting and measuring the enantiomeric excess and handedness of chiral molecules play a crucial role in chemistry, biology, and pharmacy [4–6]. As a result, development of evermore reliable methods to discern enantiomers is an ongoing quest, which has received considerable attention in recent years [7].

Experimental methods based on chiral light-matter interaction, such as Coulomb-explosion imaging [8–10], microwave spectroscopy [11,12], Raman optical activity [13,14], and laser-induced mass spectrometry [15,16], have become practice to discern enantiomers in gas phase. Moreover, ionization based photoelectron circular dichroism approaches [17–22] not only allow probing chirality in the multiphoton [23–26] and strong-field regimes [27–29], but also help us to understand molecular relaxation dynamics [30] and photoionization time delay [31]. Analogously, laser-induced photoelectron circular dichroism was recently used to obtain time-resolved chiral signal [32,33]. In particular, Beaulieu *et al.* have employed time-resolved vibronic dynamics associated with a photoexcited electronic wave packet to explain time-resolved chiral signal [32]. Recently, the signature of chirality and associated electron dynamics were also probed by chiral high-harmonic generation [34–40]. In the late 1990s, Nafie and co-workers pioneered the investigation of transition current densities in molecules [41–43]. Furthermore, current densities were already used to discern enantiomers using vibrational circular dichroism [44–46]. In most of the aforementioned methods, left- and right-circularly polarized light is used to probe chirality in gas phase for randomly orientated molecules. An alternative using pairs of linearly polarized laser pulses with skewed mutual polarizations was proposed recently [47].

Recently it has been demonstrated experimentally and theoretically that chiral molecules can be oriented in a specific direction [48,49]. When a linearly polarized laser pulse along x direction is employed, the chiral molecules will try to align themselves in such a way that the most polarizable axis in molecules will be along the x direction. There will be an equal probability of alignment along the $\pm x$ direction and molecules can rotate freely in the perpendicular plane, i.e., a chiral molecule would lie along this alignment axis and rotate about it. Orientational averaging would imply that observed signals would present no signature of chirality. A time-delayed second laser pulse with skewed polarization, linearly polarized in the xy plane at 45° between both axes, induces a dipole in the molecule. It is given by $d_i = \sum_j \alpha_{ij} E_j$, where α_{ij} is the polarizability component and E_j is the electric field component of the laser pulse. As a result of the induced dipole, a torque $\vec{\tau} = \vec{d} \times \vec{E}$ is induced along the aligned molecular axis. The analysis of the components of the torque yields a nonzero value of the average of the time derivative of the torque along z direction. The torque inducing this new alignment is proportional to the off-diagonal elements of the polarizability tensor. For nonchiral molecules, the off-diagonal elements have the

*jean-christophe.tremblay@univ-lorraine.fr
†gdixit@phy.iitb.ac.in

 ©2020 American Physical Society

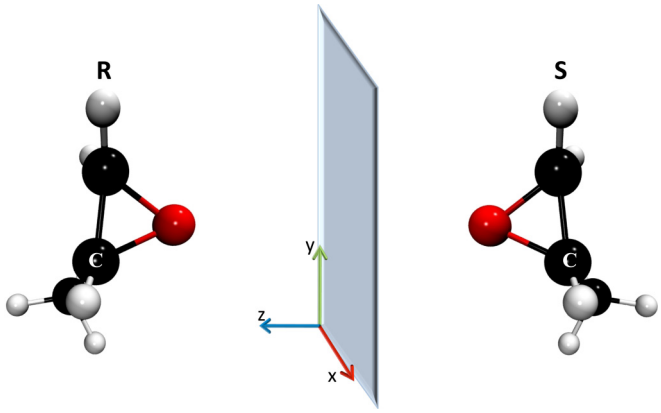

FIG. 1. R- and S-enantiomers of epoxypropane in the molecular fixed frame. Gray, black, and red spheres represent hydrogen, carbon, and oxygen atoms, respectively. The chiral carbon is labeled by C. The xy plane is the mirror plane and the normal axis lies along z direction.

same sign, so all molecules will experience the same torque. For chiral molecules, the off-diagonal elements of the polarizability tensor have opposite signs for different enantiomers. This implies that enantiomers will experience a torque in opposite directions, leading to opposite orientations, related by reflection symmetry (see Fig. 1).

On the other hand, if a circularly polarized laser pulse is applied, the interaction with the chiral molecules will be different. For $E = E_0[\cos(\omega t)\hat{x} + \sin(\omega t)\hat{y}]$, the components of the induced torque will be $\tau_x = -E_0^2[\alpha_{zx}\cos(\omega t) + \alpha_{zy}\sin(\omega t)]\sin(\omega t)$, $\tau_y = E_0^2[\alpha_{zx}\cos(\omega t) + \alpha_{zy}\sin(\omega t)]\cos(\omega t)$, and $\tau_z = -E_0^2[\alpha_{xy}\sin(\omega t) + \alpha_{yx}\cos(\omega t)]$. The average value of the z component yields zero as we analyze the above expressions. For the other components of the induced torque, even if the components are different for the enantiomers as the polarizability tensors change sign, there is no simple π-phase change relation for the enantiomers. Therefore, the interaction with a circularly polarized laser pulse can break the symmetry of the enantiomers, but unidirectional orientation cannot be achieved.

In this work we explore charge migration in chiral molecules by studying ultrafast electron dynamics induced by a linearly polarized intense laser pulse for a specific orientation of molecules, as shown in Fig. 1. It is not immediately obvious whether the electronic current density patterns in a space-fixed excited enantiomer pair should remain the same or not. The answer is encoded in the electronic current densities, which maps the direction of electron migration. According to the continuity equation, the motion of electronic charge distribution is accompanied by electronic current densities [50], which are useful to understand chemical reaction mechanisms [51–65]. The time-dependent behavior of electronic current densities in chiral molecules out-of-equilibrium remains uncharted territory. This is the main focus of our work. As will be shown below, the electronic current density can become markedly different in an enantiomer pair under specific laser-excitation conditions, which would lead to different experimental signals. To illustrate the role of time-resolved electronic current density in chiral molecules, gas phase epoxypropane (1,2-propylene oxide, see Fig. 1) is used as a realistic test system. Epoxypropane has been used in chiral high-harmonic generation [34], as well as being observed in interstellar media [66,67].

II. MODEL AND METHODS

To simulate electron dynamics in both R- and S-epoxypropane, we solve the many-electron time-dependent Schrödinger equation

$$i\partial_t \Psi(\vec{r}^N, t) = [\hat{H}_0 - \hat{\mu}\cdot\mathcal{F}(t)]\Psi(\vec{r}^N, t). \tag{1}$$

Here $\hat{H}_0$ is the field-free Hamiltonian within the Born-Oppenheimer approximation, and $\Psi(\vec{r}^N, t)$ is the time-dependent many-electron wave function for the N-electron system. The field-molecule interaction is treated in the semiclassical dipole approximation, with $\hat{\mu}$ the molecular dipole operator and $\mathcal{F}(t)$ an applied external electric field. Time-dependent configuration interaction is used to represent $\Psi(t)$ as a linear combination of the ground state Slater determinant and singly excited many-body excited states, here given in spin-free representation as

$$\Psi(\vec{r}^N, t) = \sum_{k=1}^{N_{\text{states}}} C_k(t)\Phi_k(\vec{r}^N). \tag{2}$$

Each time-independent many-electron state $\Phi_k(\vec{r}^N)$ is expressed as a linear combination of singly excited configuration state functions

$$\Phi_k(\vec{r}^N) = D_{0,k}\Phi_0(\vec{r}^N) + \sum_{ar} D^r_{a,k}\Phi^r_a(\vec{r}^N). \tag{3}$$

The configuration state functions $\Phi^r_a(\vec{r}^N)$ are spin symmetrized combinations of excited Slater determinants, which are defined from the single reference ground state Slater determinant $\Phi_0(\vec{r}^N)$ by taking an electron from an occupied molecular orbital a to a virtual molecular orbital r. In the hybrid TDDFT/CI method [68,69], the energies and the expansion coefficients $\{D_{0,k}, D^r_{a,k}\}$ of the many-body states are obtained from linear response time-dependent density functional theory.

In this work, all $N_{\text{states}} = 31$ lowest-lying excited states below the ionization threshold are used to obtain the convergence and used as a basis to represent the many-electron wave packet. They are computed using the CAM-B3LYP functional [70] and aug-cc-pVTZ basis sets [71], as implemented in Gaussian16 [72]. This combination of methods has been shown to provide a good balance between the accuracy of the electronic excited state energies as compared to benchmark wave function calculations, and a computational efficiency comparable to that configuration interaction singles [68,69]. The population dynamics were checked to be converged with respect to the number of excited states included in the wave packet expansion, by repeating the laser-driven dynamics simulations with $N_{\text{states}} = \{16, 21, 26, 31\}$. Laser-induced ionization is neglected throughout, since it would contribute only to a loss of norm of the wave packet and would consequently not further affect the coherent N-electron dynamics simulations presented here [73].

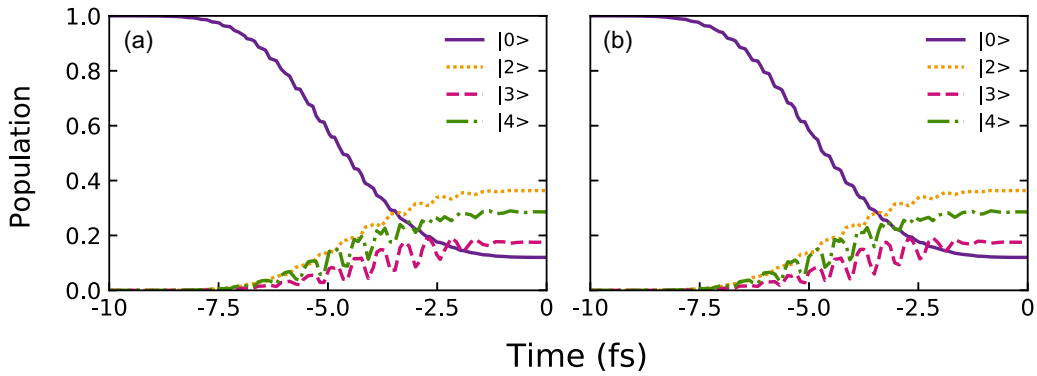

FIG. 2. Population dynamics of selected electronic states for (a) R- and (b) S-epoxypropane. A sine-squared pulse (carrier frequency: $\hbar\omega = 7.67$ eV; duration: 10 fs; peak intensity: 10.1×10^{14} W/cm^2) linearly polarized along the x axis is used to excite the first optically accessible band in both enantiomers. $|0\rangle$ represents the ground electronic state. Only the excited states at energies $E_2 = 7.51$ eV, $E_3 = 7.56$ eV, and $E_4 = 7.73$ eV are significantly populated throughout the dynamics. The time origin $\mathbf{T} = 0$ defines the onset of field-free charge migration.

From the time-dependent many-electron wave function, it is possible to recast the dynamics into a one-electron quantum continuity equation

$$\partial_t \rho(\mathbf{r}, t) = -\vec{\nabla} \cdot \mathbf{j}(\mathbf{r}, t), \tag{4}$$

where $\rho(\mathbf{r}, t)$ is the one-electron density and $\mathbf{j}(\mathbf{r}, t)$ is the electronic current density [74]. Both are obtained from the many-body wave function defined in Eqs. (2) and (3). On the one hand, the expectation value of the one-electron density operator

$$\hat{\rho}(\mathbf{r}) = \sum_k^N \delta(\mathbf{r} - \mathbf{r}_k) \tag{5}$$

allows us to calculate the one-electron density. Here $\delta(\mathbf{r} - \mathbf{r}_k)$ is the Dirac delta distribution, $\mathbf{r}$ is a point of observation, and $\mathbf{r}_k$ is the position of electron k. The flux density is similarly defined as the expectation value of the operator

$$\hat{j}(\mathbf{r}) = \frac{1}{2} \sum_k^N [\delta_k(\mathbf{r})\hat{p}_k + \hat{p}_k^\dagger \delta_k(\mathbf{r})], \tag{6}$$

where the momentum of electron k, given by operator $\hat{p}_k = -i\vec{\nabla}_k$, is respectively applied to the right and to the left in the first and second term on the right-hand side of Eq. (6). Exploiting the structure of the many-body wave function, Eqs. (2) and (3), leads to simple one-electron integrals between molecular orbitals (see Ref. [75] for details). In conventional fashion these are expressed as linear combinations of atomic orbitals, themselves expressed as combinations of atom-centered Gaussian functions. Hence, all integrals are computed analytically. It was shown in Ref. [75] that this numerical procedure yields a charge density and a current density that, taken together, very accurately satisfy the continuity equation, Eq. (4), apart from small discrepancies at the nuclei. In this work, the one-electron density and the associated electronic current density are calculated using the ORBKIT toolbox [75–77]. All dynamical simulations are performed using in-house codes [73,78–81] and the VMD software [82] is used to visualize the electronic charge distributions and associated electronic current densities. Note that current densities have interesting symmetries as illustrated in Ref. [83].

III. RESULTS AND DISCUSSION

To reveal the electron dynamics behavior of enantiomers in an external electric field, it suffices to drive the system out-of-equilibrium using a laser pulse, which transfers some population from ground electronic state to a few selected excited states. In Fig. 2 the time evolution of the many-electron state populations in the two enantiomers of epoxypropane is shown for a 10 fs sine-squared pulse linearly polarized along the x axis, with a 162 nm wavelength (7.67 eV) and 10.1×10^{14} W/cm^2 peak intensity. As evident from the figure, the state populations are identical for both enantiomers at all times. The small oscillations in the population of individual electronic states are due to the permanent dipole moments of these states, which interact with the electric field. These oscillations do not affect the population transfer dynamics. At the end of the pulse, i.e., at $\mathbf{T} = 0$, approximately 83% population is transferred from the initial ground electronic state to a coherent superposition of the second ($P_2 = 36\%$), third ($P_3 = 18\%$), and fourth ($P_4 = 29\%$) excited states. The timescales associated with different charge migration processes underlying the electron dynamics can be estimated from the energy difference between the different states populated, $\tau = h/\Delta E$. Due to significant population in the ground electronic state after the pulse, the largest energy difference of $\Delta E = 7.89$ eV leads to the fastest timescale for electron dynamics, within the attosecond regime (524 as). However, as most of the electronic population is transferred to the excited states, the dominant contribution to the electron dynamics will stem from interference effects among these three excited states. The timescale associated with these periodic processes range from 12.5 to 82.7 fs, and the electron dynamics is thus predominantly happening on the femtosecond timescale.

Although the populations are identical, it is not straightforward to infer whether the time-dependent charge distributions and associated electronic current densities [$\mathbf{j}(\mathbf{r}, t)$ in Eq. (4)] corresponding to the electronic wave packet are identical or not for both enantiomers. Figure 3(a) presents the time-dependent charge distribution differences for both enantiomers at three different times after laser excitation. The system is prepared using the pulse defined in Fig. 2 in a superposition state consisting majoritarily of the ground state and of the second, third, and fourth excited states. The charge

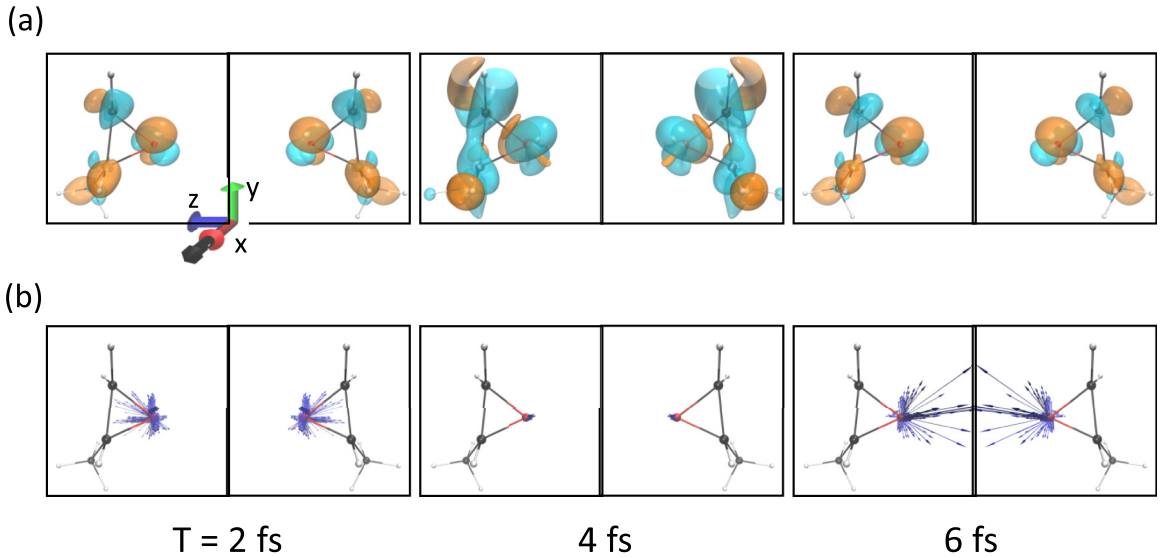

FIG. 3. (a) Charge distribution difference $\rho(\mathbf{r}, t) - \rho(\mathbf{r}, 0)$ and (b) corresponding electronic current densities (blue arrows) for both the R- and S-enantiomers during field-free charge migration, at different times after the laser pulse is polarized along the x axis. The field parameters are defined in the caption of Fig. 2. Orange and blue colors represent isosurface values of -0.0015 and $+0.0015$, respectively.

distribution at the onset of field-free charge migration (i.e., at $\mathbf{T} = 0$) is subtracted from the charge distributions at later times to help reveal the electron dynamics. At all times, the charge distribution differences for the enantiomers form mirror images, and the chirality of the enantiomer pair is preserved (see Fig. 3). The charge distribution at time $\mathbf{T} = 6$ fs is also found to be approximately similar to the distribution at $\mathbf{T} = 2$ fs. This is indicative of a partial recurrence in the dynamics. Because the electronic wave packet is a superposition of many states with incommensurate energy differences, complete recurrence is not possible. Interestingly, the oscillations in the charge distribution do not appear to involve the chiral carbon atom (see also Fig. 1). This is due to the fact that all states excited by the chosen pulse do not involve strong reorganization of the electron density close to the chiral center. Prominent charge migration is taking place only around the oxygen atom. Negative isocontour values (orange), corresponding to electron depletion, are found at time $\mathbf{T} = 2$ fs and time $\mathbf{T} = 6$ fs, where they are changed to positive isocontour values (blue) at time $\mathbf{T} = 4$ fs. There is a small change of the isocontour for other carbon atoms except chiral carbon.

The variations of the one-electron density document charge migration but it is the electronic current density $\mathbf{j}(\mathbf{r}, t)$ that yields spatially resolved mechanistic information about the processes hidden within [see Eq. (4)]. These electronic current densities are shown as blue arrows in Fig. 3(b) for the same selected snapshots as above. At all times, most of the current densities are localized around the oxygen atom. This confirms that the chiral carbon center is not involved in this particular charge migration dynamics, since many-body excited states inducing nodal structure at the chiral center are found at higher energies in epoxypropane. It is interesting to observe that the direction of the current densities have opposite phases at $\mathbf{T} = 2$ fs and $\mathbf{T} = 6$ fs, although the magnitudes are almost equal. This picture contrasts with the one offered by the charge distribution differences at these two times, which are approximately similar in particular around the top carbon atom. This phase reversal in the current densities describes a change in the flow direction of the electrons, and this information cannot be obtained from the charge distribution dynamics. Approaching this partial recurrence in the charge migration process could lead to the observed sign reversal in the flow of electrons.

Note that the charge distributions and the electronic current densities, such as the ones depicted in Fig. 3, are related by the mirror reflection for both enantiomers at all times. It is known that the mirror reflection of observables of one enantiomer along the mirror plane gives the same observable for other enantiomer due to the mirror symmetry of the chiral pair in the field. A sign change upon reflection is a fundamental measure of chirality and it is evident from Fig. 3. The general trends discussed above remain unchanged for any other field-free charge migration process in which the system is first prepared by laser pulses linearly polarized along the z axis, y axis, or for any laser polarization lying in the xy plane. In this case, the populations of electronic states will remain identical at all times for both enantiomers, whereas the time-dependent charge distributions and electronic current densities will retain the mirror symmetry of the chiral pair. This naturally brings up the question, how these results will change when we use linearly polarized pulses along a plane including z axis. Figure 4 shows the population dynamics for selected electronic states during a 10 fs sine-squared pulse of 9.1×10^{14} W/cm^2 peak intensity and 160 nm wavelength (7.75 eV). The electric field is linearly polarized at 45° between the axes in the yz plane. To achieve significant population among low-lying excited states, the pulse parameters are tuned slightly compared to the previous case. As opposed to polarization along the axes, the population dynamics for both enantiomers differ drastically. For the R-enantiomer, 50% population remains in the ground state at the end of the pulse, whereas it is 70% depleted for the S-enantiomer. The dominant state at the end of the pulse is found to be the third one ($P_3 = 32\%$ and 37% for R-

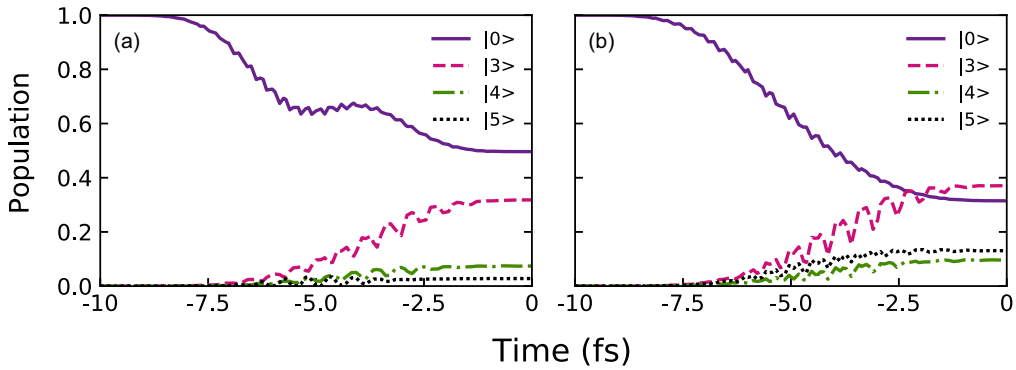

FIG. 4. Population dynamics of selected electronic states for (a) R- and (b) S-epoxypropane. A sine-squared pulse (carrier frequency: $\hbar\omega = 7.75$ eV; duration: 10 fs; peak intensity: 9.1×10^{14} W/cm^2) linearly polarized in the yz plane is used to excite the first optically accessible band in both enantiomers. Only the excited states at energies $E_3 = 7.56$ eV, $E_4 = 7.73$ eV, and $E_5 = 7.84$ eV are significantly populated throughout the dynamics.

and S-enantiomers, respectively). The latter enantiomer populates also more efficiently the fourth and fifth excited states ($P_4 = 10\%$ and $P_5 = 13\%$, respectively), providing a more democratic population distribution than in the R-enantiomer ($P_4 = 7\%$ and $P_5 = 2\%$). It appears obvious that the field-free charge migration in the two enantiomers following such linearly polarized excitation in the yz plane will be radically different.

The charge distribution differences and electronic current densities for both enantiomers are shown in Fig. 5. In this case, only contributions to the electronic wave packet stemming from the third, fourth, and fifth excited states are considered. Fast oscillating contributions from the ground state are removed. As could be inferred from the population at the pulse end, the charge migration dynamics differs drastically for the two enantiomers. Moreover, neither the charge distributions nor the electronic current densities are mirror images for both enantiomers, unlike in the case of excitation by linearly polarized pulses in the xy plane. Again, the electronic current densities are concentrated around the oxygen atom. This is confirmed by looking at the current densities [blue arrows in Fig. 5(b)], which reveals that no electrons are flowing around nor through the chiral center. As in the previous excitation scenario, the charge distributions are similar for both enantiomers at times $\mathbf{T} = 2$ and 6 fs, in particular around the oxygen atom (see Fig. 5). Although the relation to the evolution of the coherences in the system is as clear as above, the current densities are also found to be in opposite directions in these two snapshots. Apart from the huge difference in the magnitude of the current densities in the enantiomers, the nature of the evolution of the electronic current densities is also very different. At $\mathbf{T} = 2$ fs, the electronic current densities are equally distributed along z axis and x axis but at $\mathbf{T} = 4$ fs all of them are directed towards x axis and at $\mathbf{T} = 6$ fs they

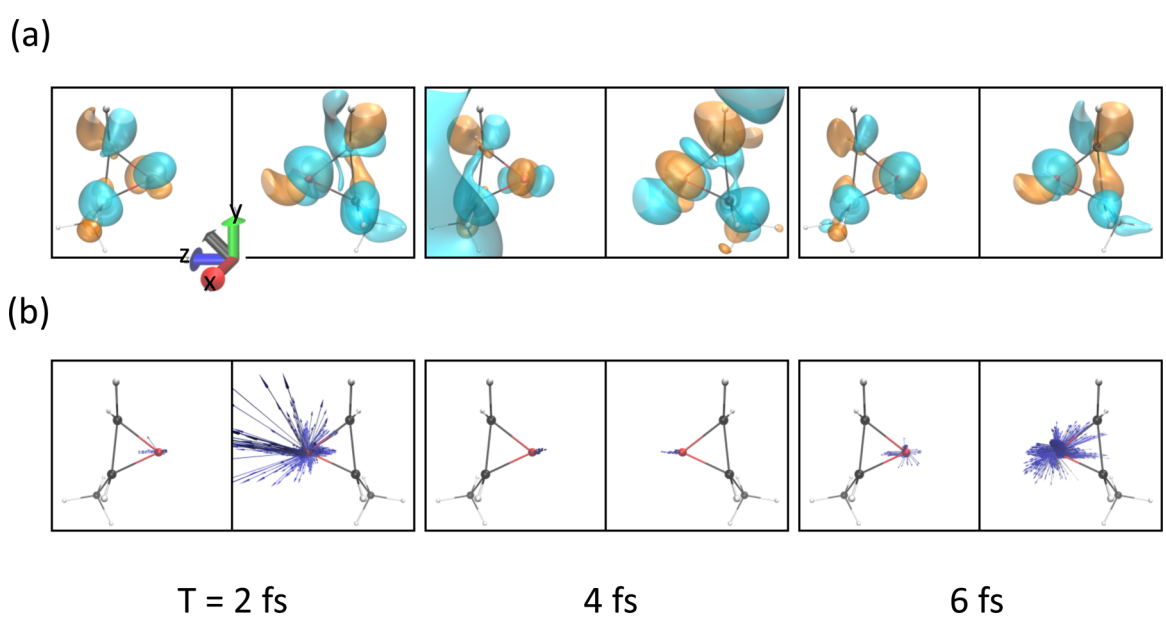

FIG. 5. (a) Charge distribution difference and (b) corresponding electronic current densities (blue arrows) for both the R- and S-enantiomers during field-free charge migration, at different times after the laser pulse is linearly polarized in the yz plane. The field parameters are defined in the caption of Fig. 4. Orange and blue colors represent isosurface values of -0.0015 and $+0.0015$, respectively.

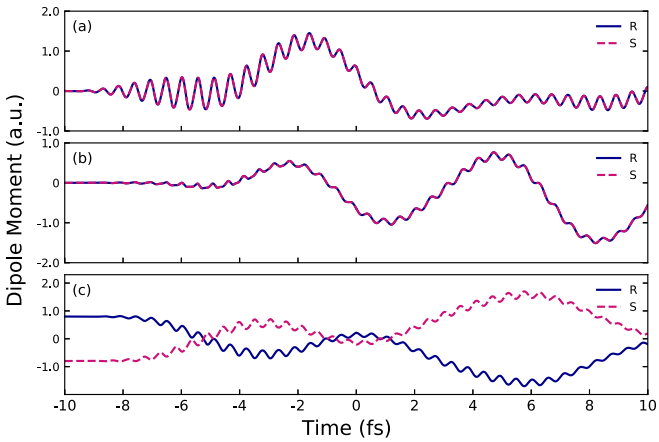

FIG. 6. Time evolution of (a) x, (b) y, and (c) z components of the total dipole moment during and after excitation by a 10 fs sine-squared pulse linearly polarized along the x axis. The field parameters are the same as in Fig. 2. Dipole moments are given in atomic units.

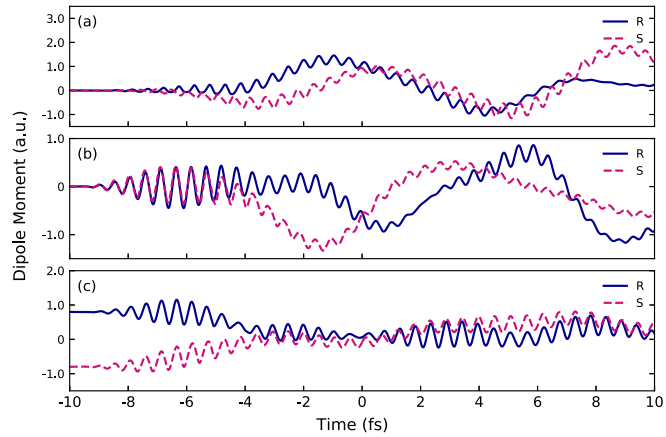

FIG. 7. Time evolution of the Cartesian components of the dipole moment along (a) x, (b) y, and (c) z directions. The amplitude and phase along all the axes are different for both enantiomers. The field parameters are the same as in Fig. 4. Dipole moments are given in atomic units.

are distributed along all the direction for the R-enantiomer. In contrast, for the S-enantiomer, at $\mathbf{T} = 2$ fs and $\mathbf{T} = 6$ fs most of the electronic current densities are distributed in the xy plane but they are directed towards the positive z axis at $\mathbf{T} = 2$ fs, whereas they are directed towards the negative z axis in later time.

The previous simulations establish unequivocally that field-free charge migration induced by linearly polarized field excitation behaves differently for laser polarizations along an axis or in the mirror xy plane than for pulses polarized in a plane including the normal axis. This laser-induced charge migration process is documented by charge distribution differences and time-dependent electronic current densities, for a specific choice of molecular orientation. Importantly, these observations remain generally valid for any orientation of the molecule, as long as the molecule retains its orientation during the laser preparation phase.

These findings cannot be applied to aligned nonchiral molecules. For example, rotating the S-enantiomer by 180° about the y axis, the rotated S-enantiomer and R-enantiomer are not the same. Consequently, the population dynamics driven by a linearly polarized pulse carefully chosen according to the prescriptions described below will be different. To explain the physical origin of the radically different current densities in enantiomer pairs, induced by linearly polarized light, time evolution of the dipole moment components for the enantiomers are calculated. The enantiomers show mirror symmetry perpendicular to the z axis in the absence of an external field (see Fig. 1). It is the presence or the absence of a mirror symmetry for the enantiomer pair in the field that determines the chirality of the electron dynamics, and this property is inherited by the subsequent field-free charge migration process.

The different Cartesian components of the total dipole moment are shown in Fig. 6 during excitation using a sine-squared pulse linearly polarized along the x axis and during subsequent field-free charge migration. The parameters of the pulse are chosen as in Fig. 2. It is evident from the figure that x and y components of the dipole moment are identical at all times for both enantiomers. On the contrary, the evolution of the z component is opposite in sign for the R- and S-enantiomers as the z axis is the chiral axis in this case (see Fig. 1). This mirror symmetry of the chiral pair can be seen by the opposite signs of the permanent dipole for the R- and S-enantiomers prior to the laser excitation, i.e., at $\mathbf{T} = -10$ fs. Upon excitation according to the first scenario, the pulse creates an electronic wave packet, which follows the mirror symmetry of the enantiomer pair. The field generates a nonuniform time-dependent electronic distribution with different projections onto the z axis. However, the electronic populations remain the same, as the orientation of the molecule relative to the xy plane is arbitrary. All linearly polarized pulses along any axis or in the xy plane will lead to a field-molecule interaction that preserves the mirror symmetry. Therefore, the x and y components of the time-evolving dipole moment will be identical for both enantiomers [see Figs. 5(a) and 5(b)]. However, the projection of the z component along the normal axis will remain the same in magnitude but opposite in phase by reflection symmetry among the enantiomers. This statement is supported by our simulations, revealing an identical behavior for the z component of the dipole moment at all times for any initial molecular orientation [see Fig. 5(c) for a specific example]. Note that the π-phase difference in chiral molecules is a very widely known phenomenon, and is also the mechanism for photoelectron circular dichroism, photoexcitation circular dichroism, microwave three wave mixing, nonlinear based chiral detection methods such as high-harmonic generation to detect chirality within the electric dipole approximation, etc. [17,19,22,32,34,35,39,47,84].

On the contrary, when the linear polarization of the pulse is rotated into a plane including the z axis and any of the two other axes, the time evolution of all components of the dipole moment is different in magnitude and phase (see Fig. 7). For a pulse linearly polarized in the yz plane, the pulse interacts coherently with the components of the dipole along both these axes simultaneously, imposing a specific phase relation among them. The relation between the y component of the dipole moment is the same for both enantiomers,

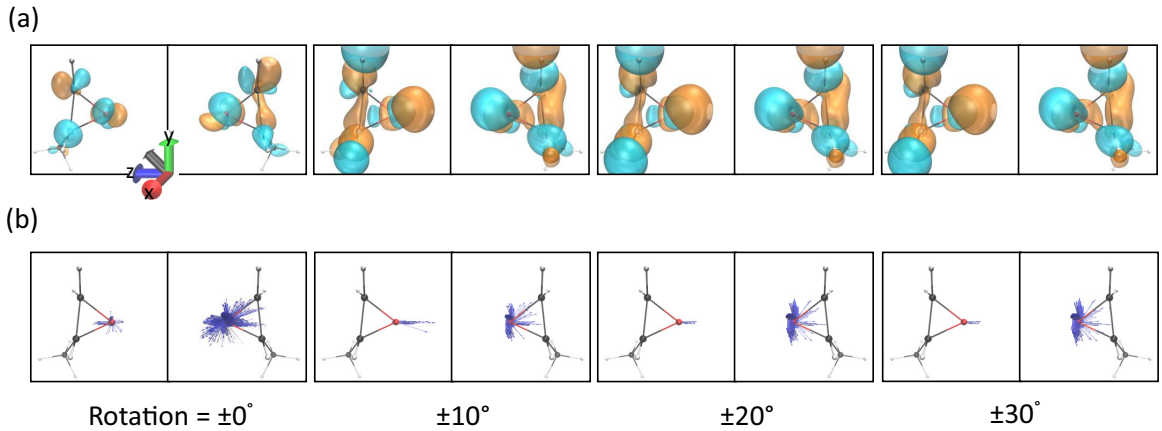

FIG. 8. (a) Charge distribution difference and (b) corresponding electronic current densities (blue arrows) for both the R- and S-enantiomers at different rotation angles with respect to the z axis, during field-free charge migration, at $\mathbf{T} = 6$ fs for a linearly polarized laser pulse in the yz plane. Isocontours at $+0.0020$ (blue) and -0.0020 (orange) for the enantiomers.

while it is of opposite phase in the z direction, therefore the torque experienced by the two enantiomers will be different. This creates a different coherent nonuniform distribution of excitations in the R- and S-enantiomers. The different populations induced by a linearly polarized pulse lead to distinct charge migration patterns, which can be mapped by the evolution of the charge distributions and by the time-dependent electronic current densities.

Till now we have discussed the electronic current densities in the oriented chiral molecule, i.e., with fixed spatial orientation. In general, most of the gas-phase methods deal with the ensembles of randomly oriented chiral molecules. Moreover, large and floppy chiral molecules are not easy to fix in the space. In the following we consider the case where a chiral molecule is not fully fixed in the space and has some uncertainty in its orientation. For this purpose we will introduce the notion of average electronic current density, which is incoherently averaged over different molecular orientations. To study the effect of orientation averaging on electronic current density for different orientations of the chiral molecule, the molecule is rotated by different angles. The absence of coherences implies an imperfect orientation in an ensemble of molecules, where each molecule has a specific orientation which might be imperfectly aligned with the laboratory-frame axes. In contrast, coherent averaging over a specific rotational quantum number would imply a complete lack of orientation of each individual molecule.

To explore the impact of imperfect orientation on the electronic current densities, we calculate the current densities at a particular time $\mathbf{T} = 6$ fs after the end of the pulse with parameters specified in Fig. 4. For this purpose we choose to investigate the electron dynamics driven by a linearly polarized laser in the yz plane. In this scenario we have flexibility to rotate the molecule in planes containing the normal axis, i.e., yz and xz planes as the z axis is our normal axis. The electronic current densities are calculated to interpret the effect of different molecular orientations. Figure 8(a) presents the charge distributions for the molecule rotated by $\pm 10^\circ$, $\pm 20^\circ$, and $\pm 30^\circ$ along the z axis at $\mathbf{T} = 6$ fs during field-free charge migration. As reflected from the figure, the charge distributions are very similar for the different values of rotational averaging. Note that the populations in the excited enantiomers change as we rotate the chiral molecule in space (not shown here).

The average current densities for larger-angle rotations are obtained by taking the average over the current densities at all smaller-angle rotations. For example, the average current densities for $\pm 30^\circ$ rotations are obtained from the current densities averaged incoherently over 0°, $\pm 10^\circ$, $\pm 20^\circ$, and $\pm 30^\circ$ rotations. The average current densities for both enantiomers are presented in Fig. 8(b). It is evident from the figure that the average current densities for $\pm 10^\circ$, $\pm 20^\circ$, and $\pm 30^\circ$ rotations are very similar, while they differ quantitatively from the current densities for the space-fixed case, i.e., 0° rotation. If we consider the current densities around individual atoms separately, say around the oxygen atom, there is a marked change in the magnitude of the current densities. The presence of a noticeable amount of current densities around chiral carbon and upper carbon atoms are very different from the current densities associated with the space-fixed molecule. The physical origin of these changes in the current densities is the variations in the phases due to the different orientations. Nonetheless, the main finding of this work remains unchanged: a linearly polarized pulse in the yz plane induces charge migration and the associated time-dependent electronic current densities are found to be different for enantiomer pairs, unrelated by mirror reflection.

IV. CONCLUSION

In summary, we have explored how time-resolved charge distributions and associated electronic current densities behave when chiral molecules are driven by linearly polarized pulses. Moreover, it is shown by means of numerical simulations that the signature of chirality in molecules can be studied by the choice of orientation in linearly polarized laser excitations, which determines how enantiomers are driven out-of-equilibrium. Our findings are valid for molecules with a fixed spatial orientation as well as for floppy molecules with an imperfect degree of orientation. It has been shown that two linearly polarized pulses can orient the chiral molecules in a

specific direction [48]. Particularly, epoxypropane and other chiral molecules can be oriented in space for sufficiently long times (of order of few picoseconds) using twisted polarization [49,85]. The enantiomers are oriented in such a manner to retain the mirror symmetry at the end of the second pulse. Our present work utilizes such oriented enantiomers while driving them out-of-equilibrium. In recent years, methods based on electric field-dipole interaction have gained importance as they provide a strong enantioselective signal [86]. Our method is different from photoexcitation circular dichroism where an enantiospecific bound electronic wave packet in a randomly oriented molecule is launched by a broadband circularly polarized pulse and a linearly polarized pulse is used to ionize the bound electronic wave packet [32]. In contrast to that, a linearly polarized pulse is used to prepare an enantiospecific bound electronic wave packet in an oriented molecule and the electronic wave packet can be probed by high-harmonic generation spectroscopy and time-resolved x-ray scattering [87]. Recently, both these methods have demonstrated the potential to probe ring currents [88] and to map electronic currents [64]. With the advent of ever faster light sources, these findings should be applicable to other chiral systems.

ACKNOWLEDGMENTS

G.D. acknowledges support from Science and Engineering Research Board (SERB) India (Project No. ECR/2017/001460). J.C.T. is thankful to the Deutsche Forschungsgemeinschaft for funding through Grant No. TR1109/2-1.

[1] J. L. Bada, Nature (London) **374**, 594 (1995).
[2] D. G. Blackmond, Cold Spring Harbor Perspect. Biol. **2**, a002147 (2010).
[3] U. J. Meierhenrich, Eur. Rev. **21**, 190 (2013).
[4] K. Mori, Chirality **23**, 449 (2011).
[5] P. Fischer and F. Hache, Chirality **17**, 421 (2005).
[6] Y. Inoue and V. Ramamurthy, *Chiral Photochemistry* (CRC, Boca Raton, FL, 2004).
[7] E. Castiglioni, S. Abbate, and G. Longhi, Chirality **23**, 711 (2011).
[8] M. Pitzer *et al.*, Science **341**, 1096 (2013).
[9] M. Pitzer *et al.*, Chem. Phys. Chem. **17**, 2465 (2016).
[10] P. Herwig *et al.*, Science **342**, 1084 (2013).
[11] D. Patterson, M. Schnell, and J. M. Doyle, Nature (London) **497**, 475 (2013).
[12] S. Eibenberger, J. Doyle, and D. Patterson, Phys. Rev. Lett. **118**, 123002 (2017).
[13] L. D. Barron, M. P. Bogaard, and A. D. Buckingham, J. Am. Chem. Soc. **95**, 603 (1973).
[14] L. D. Barron, *Molecular Light Scattering and Optical Activity* (Cambridge University Press, Cambridge, 2009).
[15] A. Bornschlegl, C. Logé, and U. Boesl, Chem. Phys. Lett. **447**, 187 (2007).
[16] R. Li, R. Sullivan, W. Al-Basheer, R. M. Pagni, and R. N. Compton, J. Chem. Phys. **125**, 144304 (2006).
[17] C. J. Harding, Ph.D. thesis, University of Nottingham, 2005.
[18] N. Böwering, T. Lischke, B. Schmidtke, N. Müller, T. Khalil, and U. Heinzmann, Phys. Rev. Lett. **86**, 1187 (2001).
[19] L. Nahon, G. A. Garcia, C. J. Harding, E. Mikajlo, and I. Powis, J. Chem. Phys. **125**, 114309 (2006).
[20] M. H. M. Janssen and I. Powis, Phys. Chem. Chem. Phys. **16**, 856 (2014).
[21] B. Ritchie, Phys. Rev. A **13**, 1411 (1976).
[22] I. Powis, J. Chem. Phys. **112**, 301 (2000).
[23] C. Lux *et al.*, Angew. Chem. Int. Ed. **51**, 5001 (2012).
[24] C. S. Lehmann, N. B. Ram, I. Powis, and M. H. M. Janssen, J. Chem. Phys. **139**, 234307 (2013).
[25] C. Lux, M. Wollenhaupt, C. Sarpe, and T. Baumert, Chem. Phys. Chem. **16**, 115 (2015).
[26] S. Beaulieu *et al.*, Faraday Discuss. **194**, 325 (2016).
[27] I. Dreissigacker and M. Lein, Phys. Rev. A **89**, 053406 (2014).
[28] S. Beaulieu *et al.*, New J. Phys. **18**, 102002 (2016).
[29] S. Rozen *et al.*, Phys. Rev. X **9**, 031004 (2019).
[30] A. Comby *et al.*, J. Phys. Chem. Lett. **7**, 4514 (2016).
[31] S. Beaulieu *et al.*, Science **358**, 1288 (2017).
[32] S. Beaulieu *et al.*, Nat. Phys. **14**, 484 (2018).
[33] A. G. Harvey, Z. Mašín, and O. Smirnova, J. Chem. Phys. **149**, 064104 (2018).
[34] R. Cireasa *et al.*, Nat. Phys. **11**, 654 (2015).
[35] O. Smirnova, Y. Mairesse, and S. Patchkovskii, J. Phys. B: At. Mol. Opt. Phys. **48**, 234005 (2015).
[36] D. Wang *et al.*, Opt. Express **25**, 23502 (2017).
[37] Y. Harada, E. Haraguchi, K. Kaneshima, and T. Sekikawa, Phys. Rev. A **98**, 021401(R) (2018).
[38] D. Baykusheva and H. J. Wörner, Phys. Rev. X **8**, 031060 (2018).
[39] O. Neufeld, D. Ayuso, P. Decleva, M. Y. Ivanov, O. Smirnova, O. Cohen, Phys. Rev. X **9**, 031002 (2019).
[40] D. Baykusheva *et al.*, PNAS **116**, 23923 (2019).
[41] L. A. Nafie, J. Phys. Chem. A **101**, 7826 (1997).
[42] T. B. Freedman *et al.*, J. Phys. Chem. A **102**, 3352 (1998).
[43] T. B. Freedman, M. L. Shih, E. Lee, and L. A. Nafie, J. Am. Chem. Soc. **119**, 10620 (1997).
[44] M. Fusè, F. Egidi, and J. Bloino, Phys. Chem. Chem. Phys. **21**, 4224 (2019).
[45] G. Magyarfalvi, G. Tarczay, and E. Vass, Wiley Interdiscip. Rev. Comput. Mol. **1**, 403 (2011).
[46] T. B. Freedman, E. Lee, and L. A. Nafie, J. Phys. Chem. A **104**, 3944 (2000).
[47] A. Yachmenev and S. N. Yurchenko, Phys. Rev. Lett. **117**, 033001 (2016).
[48] I. Tutunnikov, E. Gershnabel, S. Gold, and I. S. Averbukh, J. Phys. Chem. Lett. **9**, 1105 (2018).
[49] I. Tutunnikov, J. Floß, E. Gershnabel, P. Brumer, I. S. Averbukh, A. A. Milner, and V. Milner, Phys. Rev. A **101**, 021403(R) (2020).
[50] J. J. Sakurai, *Advanced Quantum Mechanics* (Pearson Education, India, 1967).
[51] I. Barth and J. Manz, Angew. Chem. Int. Ed. **45**, 2962 (2006).
[52] I. Barth, J. Manz, Y. Shigeta, and K. Yagi, J. Am. Chem. Soc. **128**, 7043 (2006).

[53] K. Nagashima and K. Takatsuka, J. Phys. Chem. A **113**, 15240 (2009).
[54] M. Okuyama and K. Takatsuka, Chem. Phys. Lett. **476**, 109 (2009).
[55] D. J. Diestler, A. Kenfack, J. Manz, and B. Paulus, J. Phys. Chem. A **116**, 2736 (2011).
[56] K. Takatsuka and T. Yonehara, Phys. Chem. Chem. Phys. **13**, 4987 (2011).
[57] S. Patchkovskii, J. Chem. Phys. **137**, 084109 (2012).
[58] M. Okuyama and K. Takatsuka, Bull. Chem. Soc. Jpn. **85**, 217 (2012).
[59] D. J. Diestler *et al.*, J. Phys. Chem. A **117**, 8519 (2013).
[60] K. Takatsuka, T. Yonehara, K. Hanasaki, and Y. Arasaki, *Chemical Theory beyond the Born-Oppenheimer Paradigm: Nonadiabatic Electronic and Nuclear Dynamics in Chemical Reactions* (World Scientific, Singapore, 2015).
[61] G. Hermann, B. Paulus, J. F. Pérez-Torres, and V. Pohl, Phys. Rev. A **89**, 052504 (2014).
[62] K. Yamamoto and K. Takatsuka, Chem. Phys. Chem. **16**, 2534 (2015).
[63] G. Hermann *et al.*, J. Phys. Chem. A **120**, 5360 (2016).
[64] G. Hermann, V. Pohl, G. Dixit, and J. C. Tremblay, Phys. Rev. Lett. **124**, 013002 (2020).
[65] T. Bredtmann, M. Ivanov, and G. Dixit, Nat. Commun. **5**, 5589 (2014).
[66] B. A. McGuire *et al.*, Science **352**, 1449 (2016).
[67] A. Bergantini *et al.*, Astrophys. J. **860**, 108 (2018).
[68] S. Klinkusch and J. C. Tremblay, J. Chem. Phys. **144**, 184108 (2016).
[69] G. Hermann and J. C. Tremblay, J. Chem. Phys. **145**, 174704 (2016).
[70] T. Yanai, D. Tew, and N. Handy, Chem. Phys. Lett. **393**, 51 (2004).
[71] J. Dunning and H. Thom, J. Chem. Phys. **90**, 1007 (1989).
[72] M. J. Frisch *et al.*, Gaussian 16, Revision C.01, Gaussian Inc., Wallingford CT (2016).
[73] J. C. Tremblay, S. Klinkusch, T. Klamroth, and P. Saalfrank, J. Chem. Phys. **134**, 044311 (2011).
[74] I. Barth *et al.*, Chem. Phys. Lett. **481**, 118 (2009).
[75] V. Pohl, G. Hermann, and J. C. Tremblay, J. Comput. Chem. **38**, 1515 (2017).
[76] G. Hermann *et al.*, J. Comput. Chem. **37**, 1511 (2016).
[77] G. Hermann, V. Pohl, and J. C. Tremblay, J. Comput. Chem. **38**, 2378 (2017).
[78] J. C. Tremblay and T. Carrington Jr., J. Chem. Phys. **121**, 11535:1 (2004).
[79] J. C. Tremblay, T. Klamroth, and P. Saalfrank, J. Chem. Phys. **129**, 084302:1 (2008).
[80] J. C. Tremblay and P. Saalfrank, Phys. Rev. A **78**, 063408 (2008).
[81] J. C. Tremblay, P. Krause, T. Klamroth, and P. Saalfrank, Phys. Rev. A **81**, 063420 (2010).
[82] W. Humphrey, A. Dalke, and K. Schulten, J. Mol. Graph. **14**, 33 (1996).
[83] A. D. Bandrauk, J. Guo, and K. J. Yuan, J. Opt. **19**, 124016 (2017).
[84] M. Leibscher, T. F. Giesen, and C. P. Koch, J. Chem. Phys. **151**, 014302 (2019).
[85] A. A. Milner, J. A. M. Fordyce, I. MacPhail-Bartley, W. Wasserman, V. Milner, I. Tutunnikov, and I. S. Averbukh, Phys. Rev. Lett. **122**, 223201 (2019).
[86] A. F. Ordonez and O. Smirnova, Phys. Rev. A **98**, 063428 (2018).
[87] G. Dixit, O. Vendrell, and R. Santra, Proc. Natl. Acad. Sci. **109**, 11636 (2012).
[88] O. Neufeld and O. Cohen, Phys. Rev. Lett. **123**, 103202 (2019).